

Article

Experimental Investigation and Artificial Neural Network Based Prediction of Bond Strength in Self-Compacting Geopolymer Concrete Reinforced with Basalt FRP Bars

Sherin Khadeeja Rahman * and Riyadh Al-Ameri 

School of Engineering, Deakin University, Geelong, VIC 3216, Australia; r.alameri@deakin.edu.au

* Correspondence: skrahman@deakin.edu.au

Abstract: The current research on concrete and cementitious materials focuses on finding sustainable solutions to address critical issues, such as increased carbon emissions, or corrosion attack associated with reinforced concrete structures. Geopolymer concrete is considered to be an eco-friendly alternative due to its superior properties in terms of reduced carbon emissions and durability. Similarly, the use of fibre-reinforced polymer (FRP) bars to address corrosion attack in steel-reinforced structures is also gaining momentum. This paper investigates the bond performance of a newly developed self-compacting geopolymer concrete (SCGC) reinforced with basalt FRP (BFRP) bars. This study examines the bond behaviour of BFRP-reinforced SCGC specimens with variables such as bar diameter (6 mm and 10 mm) and embedment lengths. The embedment lengths adopted are 5, 10, and 15 times the bar diameter (d_b), and are denoted as $5 d_b$, $10 d_b$, and $15 d_b$ throughout the study. A total of 21 specimens, inclusive of the variable parameters, are subjected to direct pull-out tests in order to assess the bond between the rebar and the concrete. The result is then compared with the SCGC reinforced with traditional steel bars, in accordance with the ACI 440.3R-04 and CAN/CSA-S806-02 guidelines. A prediction model for bond strength has been proposed using artificial neural network (ANN) tools, which contributes to the new knowledge on the use of Basalt FRP bars as internal reinforcement in an ambient-cured self-compacting geopolymer concrete.

Keywords: self-compacting geopolymer concrete; basalt; fibre-reinforced polymer; pull-out test; bond strength prediction; ANN model



Citation: Rahman, S.K.; Al-Ameri, R. Experimental Investigation and Artificial Neural Network Based Prediction of Bond Strength in Self-Compacting Geopolymer Concrete Reinforced with Basalt FRP Bars. *Appl. Sci.* **2021**, *11*, 4889. <https://doi.org/10.3390/app11114889>

Academic Editor: Dario De Domenico

Received: 8 April 2021

Accepted: 25 May 2021

Published: 26 May 2021

Publisher's Note: MDPI stays neutral with regard to jurisdictional claims in published maps and institutional affiliations.



Copyright: © 2021 by the authors. Licensee MDPI, Basel, Switzerland. This article is an open access article distributed under the terms and conditions of the Creative Commons Attribution (CC BY) license (<https://creativecommons.org/licenses/by/4.0/>).

1. Introduction

The construction industry today is heavily focused on the use of durable and sustainable construction materials for major infrastructural developments, owing to increased repair and maintenance expenses [1]. The service life of reinforced structures is considered significant when used in aggressive or marine environments. Hence, these structures need to be corrosion proof and durable in terms of structural performance [2]. In traditional construction practices involving the use of cement, a large amount of carbon dioxide emission occurs, and they are also energy intensive. Therefore, it has become necessary to adopt alternate construction materials which are sustainable and durable at the same time. The use of sustainable geopolymer concrete in conjunction with fibre-reinforced polymer (FRP) bars ought to resolve the corrosion issues of traditional reinforced structures [3]. However, in order to achieve wider acceptance for this novel composite structure, it is necessary to investigate the serviceability properties of FRP-reinforced concrete structures, including factors such as deflections and crack widths [1,3]. The formation of crack width and deflections is often governed by the reinforcement bar spacing and bond behaviour [4,5]; this necessitates the need for more studies on the bond behaviour of the newly developed composite.

Advanced research on using combustion by-products from power plants, including fly ash and slag, as cementitious materials has resulted in the development of self-compacting geopolymer concrete (SCGC), which can be cured under ambient conditions and is very

much suitable for structures involving dense reinforcements [6–8]. The quality of concrete, especially when using self-compacting concretes (SCCs), may be of significance, since the composition of SCCs with higher fines contents and lower amounts of coarse aggregates may affect the shear capacity of the specimens under consideration [9,10]. It is reported that unlike conventional concrete, self-compacting concrete may cause an accumulation of water when used in reinforced structures, due to bleeding and segregation.

Furthermore, research on producing corrosion-resistant materials has resulted in the development of reinforcement bars made of fibre-reinforced polymers, known as fibre-reinforced polymer (FRP) bars. Different FRP bars, such as glass FRP (GFRP), carbon FRP (CFRP), basalt FRP (BFRP), and aramid FRP (AFRP), are now commercially available, and are being used in aggressive environments owing to their superior durability properties in comparison to conventional steel reinforcement [11,12]. FRP bars are generally produced by pultrusion of the polymer fibre bundles held together by the use of various resins or epoxies [2]. Even though FRP bars are durable, lightweight, and stronger compared to conventional steel reinforcement, the wider application of these bars is limited due to the lack of research on their wider properties, including those relating to bond behaviour—specifically, bonding with concrete and structural performance [13–15]. Unlike other FRP bars, basalt FRP bars are cost effective and weather resistant in comparison with the widely used glass FRP bars [16].

To promote the wider use of this newer composite construction material, research needs to be conducted on the holistic aspects of structural properties. Current design practices consider the knowledge of bond properties to govern the serviceability and ultimate capacity requirements of reinforced structures [17–19]. Unlike steel bars, FRP bars are anisotropic, reporting a different pull-out and failure type in comparison with steel bars [20]. It is also to be noted that the bond behaviour of FRP bars in any type of concrete is governed by various factors, including rebar stiffness, rebar surface type, grade of concrete, types of resins used, and volume of fibre bundles in the FRP bars [1,17]. Knowledge of bond properties is also required for computing the development lengths of the reinforced structures [10,21].

In this paper, direct pull-out tests have been carried out in order to study the bond strength of basalt FRP bars reinforcing a newly developed self-compacting geopolymer concrete (SCGC) [8]. The variables used in this study are bar diameter and embedment length. The test results compile the influence of bar diameter and embedment length on bond strength, failure type, and calculation of development length. Based on the outcomes from the experimental investigation, a prediction model has been developed for the bond strength and anchorage length of the BFRP-reinforced SCGC specimens.

2. Experimental Investigation

The experimental program consisted of direct pull-out tests on composite specimens of BFRP–SCGC and Steel–SCGC. Compared to the bond beam test, the direct pull-out test is the simplest and most efficient as per the ACI440.3R-04 [22] and RILEM recommendations [23]. This study will investigate the effects of bar diameter and embedment length on the bond behaviour of the pull-out specimens made of BFRP- and steel bar-reinforced SCGC. The tests conducted on the specimens, after 28 days of curing, will evaluate the effects of the above-mentioned parameters on the maximum pull-out load and, thereby, the bond strength, of the composites under investigation.

2.1. Test Program

The test program consisted of pull-out tests on SCGC specimens reinforced with BFRP and steel bars. The test variables were the bar embedment lengths ($5 d_b$, $10 d_b$, $15 d_b$) and bar diameters (6 mm, 10 mm) of the basalt FRP bars, aiming to assess their effects on the bond behaviour with SCGC. Thus, three pull-out specimens were cast for each configuration, along with the specimens made of SCGC with steel bars for comparison purposes. The reinforcement bars were of 400 mm length and the SCGC cubes were of

150 mm × 150 mm × 150 mm size. A total of 21 specimens were designed for the experimental investigation; the parameters were selected in such a way that the desired failure would be of pull-out type, ensuring accurate depiction of the bond stress distribution and bond strength development.

2.2. Materials

Two types of reinforcing bars—namely, basalt FRP, and steel bars—are used in this study. The basalt fibre-reinforced polymer (BFRP) bars were provided by Jiangsu Oceanpower New Material Technology Co., Zhenjiang, China. The BFRP bars were produced via a pultrusion process, in which the continuous basalt fibres were embedded in an epoxy resin with minimal fibre volume. The bars used in the study were 400 mm long, with two bar diameters of 6 mm and 10 mm, and a spiral-wound surface. The steel rebars used in this study were 10 mm deformed steel bars from a local manufacturer.

The mechanical properties of the BFRP and steel bars were previously compared by the second author [24] in a study on the bond behaviour of basalt FRP bars in normal concrete. The material properties of the BFRP bars were then cross-checked against those given by the manufacturer at Deakin's testing facility [24]. The test results confirmed the values provided by the manufacturer, and the results are detailed in Table 1 below.

Table 1. Mechanical properties of BFRP and steel bars [1].

Bar Type	Nominal Diameter (mm)	Tensile Strength (MPa)	Elastic Modulus (GPa)
BFRP	6	1000	≥55
BFRP	10	1260	≥55
Steel	10	620	200

The steel bars and the basalt FRP bars used in this study are also shown in Figure 1 below:



Figure 1. Basalt FRP and steel pull-out bars used in this study.

The concrete used in this study is a 40 MPa novel ambient-cured self-compacting geopolymer concrete (SCGC) developed by the authors [8]. The SCGC, which was produced in the Structures Laboratory at Deakin University's Geelong Waurm Ponds Campus, exhibits self-compacting properties and eliminates the need for compaction and vibration of the specimens [9,25,26]. The newly developed SCGC consists of fly ash, slag, and micro fly ash as binder materials and anhydrous sodium metasilicate as an alkali activator, along with fine and coarse aggregates without use of any superplasticisers. The fly ash and micro fly ash for the SCGC are sourced from Cement Australia and Fly Ash Australia, respectively. Also, the slag and sodium metasilicate are sourced from Independent Cements and Redox, Melbourne, Australia respectively.

The mixing and casting of the SCGC was carried out using the same procedure as mentioned in the previous study by the authors [8]. The mixing, casting, and curing of the pull-out specimens was carried out in laboratory environmental conditions of 23 ± 2 °C at a relative humidity of 50% in Deakin University's Geelong Waurin Ponds Campus. Prior to casting, the fresh properties of the SCGC were determined using the slump flow and T500 tests. In this study, 12 additional cylinders (200 mm × 100 mm) were prepared from the same batch of SCGC in order to determine the mechanical properties after 28 days of curing under ambient conditions. The additional cylinders will help in confirming the mechanical properties of the pull-out specimens. The mix proportion and average strength characteristics of the SCGC used in this study are given in Table 2 below [8]:

Table 2. Mix proportion and properties of self-compacting geopolymer concrete.

Mix Proportion (Kg/m ³) [2]	
Fly Ash	480
Slag	360
Micro Fly Ash	120
Sodium Metasilicate (Anhy.) Alkali Activator	96
Fine Aggregates	763
Coarse Aggregates	677
Properties of Fresh SCGC	
Slump Flow (mm)	670
T500 (sec)	4.10
Properties of Hardened SCGC	
Compressive Strength, at 28th Day (MPa)	40
Indirect Tensile Strength, at 28th Day (MPa)	3
Modulus of Elasticity, at 28th Day (GPa)	15

A laboratory pan mixer with a maximum capacity of 200 kg was used for the mixing of the SCGC, and the slump flow and T500 of the SCGC mix were tested using an Abrams Cone. The slump flow of the current SCGC mix is shown in Figure 2 below:



Figure 2. Slump flow of SCGC.

2.3. Pull-Out Specimen Preparation

The direct pull-out test was carried out in accordance with the ACI 440.3R-04 and CSA-S806-02 standard guidelines. A 150 mm cubic mould was used to prepare the pull-out specimens. The moulds were prepared by partitioning rectangular steel moulds with plywood formwork supported by clamps, as shown in Figure 3.

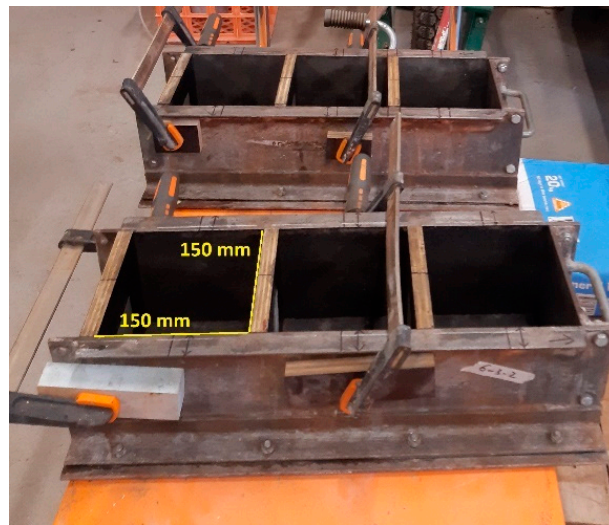


Figure 3. Moulds for pull-out specimens.

Prior to the preparation of the cubic moulds, the basalt FRP bars were marked and fixed in the steel socket using a strong adhesive named HILTI RE500 for better grip in the socket, unlike the conventional cement grout method. The use of an epoxy adhesive of this kind will prevent the failure of FRP bars due to the gripping force of the clamps in the universal testing machine during testing [3]. The basalt FRP bars gripped in the steel socket tubes were left to dry for one week. The embedment length, also known as the bonded length or bond length, was determined with respect to the reinforcing bar's diameter. The three embedment lengths used in this study were the $5 d_b$, $10 d_b$, and $15 d_b$ lengths. The embedment length of $5 d_b$ corresponds to a bonded length equal to 5 times the diameter of the bar. Later, the embedment lengths were marked on the basalt FRP bars, and the unbonded lengths were taped using foams as bond breakers and made ready for casting in the cubic moulds (Figure 4).



Figure 4. Pull-out bars taped with bond breaker foams before casting.

A day before casting, the steel cubic moulds were cleaned, and a natural release agent called LanoForm was applied. Later, the prepared basalt FRP and steel bars were placed at the bottom of the mould and clamped on either side of the mould to prevent slippage from the centre of the mould. On the day of casting, the freshly prepared SCGC was poured, with the pull-out bars in the centre of the mould (Figure 5).



Figure 5. Pull-out specimens filled with SCGC.

The pull-out specimens were then demoulded and subjected to ambient curing for 28 days by leaving them in the laboratory at a room temperature of 23 ± 2 °C and at a relative humidity of 50%. The demoulded specimens on the day of testing are shown in Figure 6 below:



Figure 6. Pull-out specimens after 28 days of curing.

2.4. Pull-Out Test Set-Up

The test method for a direct pull-out test considers two widely accepted standards of testing on FRP-reinforced structures—namely, ACI 440.3R-04 [22], and CAN/CSA-S806-02 [27]. The test procedures outlined in both standards are very similar, with a minor variation in the maximum loading rate, where a 1.3 mm/min maximum is mentioned in the former, whereas a maximum of 1.27 mm/min is suggested in the latter. The pull-out test in this study was carried out using a 300 kN Instron universal testing machine in the Deakin University Structures Laboratory at Geelong Waurn Ponds Campus. The loading rate applied to the steel and basalt FRP bars was 1 mm/min, and was measured using the automated data acquisition system of the machine. The pull-out specimen cube embedded with basalt FRP was placed and tightened in a steel frame fitted in the testing machine, as seen in Figure 7.



Figure 7. Universal testing machine with automated data acquisition system for pull-out testing.

The steel frame consisted of bottom and top steel plates with holes on all four sides and in the centre, allowing for the FRP bar to pass through. The bottom plate of the steel frame was connected to the jaws of the testing machine, and acted as the reaction end when the pull-out load was resisted by the specimen under testing, as seen in Figure 8.

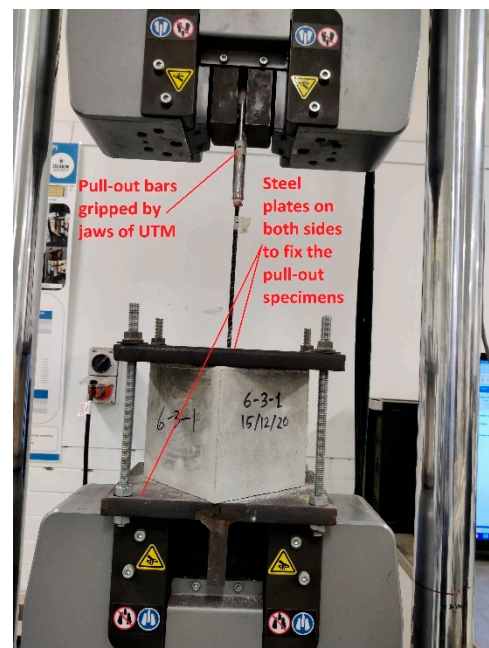


Figure 8. Placing of the pull-out specimen inside the UTM.

The applied load was recorded by the data acquisition system and connected to the computer. During the loading, the slip of the basalt FRP bar corresponding to the applied load was measured continuously and recorded in the Bluehill software mod-

ule of the Instron universal testing machine. The tests were run until failure for each individual specimen.

The pull-out specimens are labelled according to the bar diameter and embedment length; for example, in the specimen named 6-1-1, 6 corresponds to a pull-out specimen of 6 mm diameter basalt FRP, 1 corresponds to an embedment length of 5 times the bar diameter (d_b), and 1 signifies the 1st specimen of similar configuration. Similarly, for pull-out specimens with steel reinforcement bars, the label is S-10-1, where S corresponds to the steel bar, 10 is the bar diameter, and 1 signifies the 1st specimen of similar configuration. In the case of steel specimens, only one embedment length of 50 mm—corresponding to $5 d_b$ —was used, since the failure mode was already established as being of the pull-out type by existing literature. The pull-out test was carried out on 3 identical pull-out specimens of each configuration, totalling 21 specimens. The specimen details and their corresponding bar diameters and bond lengths are depicted in Table 3 below:

Table 3. Specimen naming and identification details.

Sl. No	Specimen No.	Bar Diameter d_b (mm)	Embedment Length in Terms of Bar Diameter	Embedment Length (mm)
1	6-1-1	6	$5 d_b$	30
2	6-1-2	6	$5 d_b$	30
3	6-1-3	6	$5 d_b$	30
4	6-2-1	6	$10 d_b$	60
5	6-2-2	6	$10 d_b$	60
6	6-2-3	6	$10 d_b$	60
7	6-3-1	6	$15 d_b$	90
8	6-3-2	6	$15 d_b$	90
9	6-3-3	6	$15 d_b$	90
10	10-1-1	10	$5 d_b$	50
11	10-1-2	10	$5 d_b$	50
12	10-1-3	10	$5 d_b$	50
13	10-2-1	10	$10 d_b$	100
14	10-2-2	10	$10 d_b$	100
15	10-2-3	10	$10 d_b$	100
16	10-3-1	10	$15 d_b$	150
17	10-3-2	10	$15 d_b$	150
18	10-3-3	10	$15 d_b$	150
19	S-10-1	10	$5 d_b$	50
20	S-10-2	10	$5 d_b$	50
21	S-10-3	10	$5 d_b$	50

3. Test Results and Discussion

In this study, the impact of various parameters—such as reinforcement bar type, bar diameter, embedment length, and concrete material—on bond behaviour are discussed. In the direct pull-out test, the bond stress of reinforcing bars and concrete is assumed to act evenly along the bond length. The following sections discuss the bond behaviour of the BFRP- and steel-reinforced SCGC with respect to the above-mentioned parameters. It is significant to note that the predominant type of failure in this study is the pull-out failure of specimens. This can be attributed to the sufficiently thick concrete cover provided to the pull-out specimens [3].

The pull-out tests were conducted on all specimens after curing under ambient conditions for 28 days. For all of the specimens, the failure type was by pull-out of the rebars. The maximum bond stress (τ_{\max}) is calculated as:

$$\tau_{\max} = P_{\max} / \pi d_b L \quad (1)$$

where, P_{\max} is the maximum pull-out force on the rebar, d_b is the bar diameter, and L is the embedment length as per the CSA -S806-02 and ACI 440.3R-04 standards.

The characteristic bond strength (τ_{\max}) is calculated as the mean of the maximum bond stress of three identical specimens of each configuration.

3.1. Bond Strength

The direct pull-out test conducted in this study consisted of testing and reporting the failure load, mode of failure, bond strength, and the load–slip relationship for each test. The bond strength, which is a critical factor in assessing the bond behaviour, is calculated using Equation (1), above. The failure load and the corresponding bond strength of the various test specimens are detailed in Table 4, below:

Table 4. Experimental results of the pull-out test specimens.

Sl.No	Specimen No	Bar Diameter, d_b (mm)	Embedment Length	Max. Load at Failure, P_{\max} (N)	Bond Stress, τ_{\max} (MPa)	Average Bond Stress, τ_{\max}^{*a} (MPa)	Standard Error of Mean	Mode of Failure
1	6-1-1	6	5 d_b	1313.21	2.32			Pull-out
2	6-1-2	6	5 d_b	5849.67	10.34 #	3.30	2.41	Pull-out
3	6-1-3	6	5 d_b	2420.91	4.28			Pull-out
4	6-2-1	6	10 d_b	4337.71	3.84			Pull-out
5	6-2-2	6	10 d_b	3120.17	2.76	3.49	0.36	Pull-out
6	6-2-3	6	10 d_b	4388.16	3.88			Pull-out
7	6-3-1	6	15 d_b	14,529.08	8.56			Pull-out
8	6-3-2	6	15 d_b	11,161.75	6.58	7.57	1.68	Pull-out
9	6-3-3	6	15 d_b	4803.68	2.83 #			Pull-out
10	10-1-1	10	5 d_b	14,195.87	9.04			Pull-out
11	10-1-2	10	5 d_b	18,504.16	11.78	9.98	0.90	Pull-out
12	10-1-3	10	5 d_b	14,318.88	9.12			Pull-out
13	10-2-1	10	10 d_b	21,830.84	6.95			Pull-out
14	10-2-2	10	10 d_b	15,498.56	4.93	6.86	1.09	Pull-out
15	10-2-3	10	10 d_b	27,340.62	8.70			Pull-out
16	10-3-1	10	15 d_b	25,295.03	5.37			Pull-out ^{*b}
17	10-3-2	10	15 d_b	25,947.93	5.51	5.41	0.05	Pull-out ^{*b}
18	10-3-3	10	15 d_b	25,180.94	5.34			Pull-out ^{*b}
19	S-10-1	10	5 d_b	9066.53	5.77 #			Pull-out
20	S-10-2	10	5 d_b	21,528.76	13.71	13.93	2.72	Pull-out
21	S-10-3	10	5 d_b	22,234.29	14.15			Pull-out

^{*a}: The average value of the bond strength of specimens of the same configuration. ^{*b}: Pull-out of bars from the specimen which was then followed by cracking of the concrete. #: These values were reported due to faulty running of the machine during the testing time, and were discarded for the average bond strength calculation.

From the bond test results, it is evident that the average bond strength of the steel-reinforced self-compacting geopolymer specimens is greater than that of the basalt FRP-

reinforced specimens. It can be observed that at the same embedment length of $5 d_b$, BFRP behaved like steel bar, reporting almost 72% of the bond strength of steel. The higher bond strength exhibited by steel bars can be attributed to the higher axial stiffness and ribbed surface of the steel bars in comparison to the basalt FRP bars [3]. In this study, the 6-mm BFRP bars reported a lower bond strength, where the bars pulled out earlier due to the greater ultimate tensile strength of the bars in comparison with the bonding force between the bars and the surrounding concrete, as reported in a study by Wang et al. [28]. This observation confirms the outcomes from the 2018 study by Nguyen et al., where the reported bond strength was 1 MPa [29]. This implies that in the case of deformed steel bars, the bonding resistance of concrete is governed by shear-based resistance, while it is friction-based for the basalt bars [29,30].

However, for the 10-mm BFRP bars, the trend was consistent with the widely reported literature, where an increase in the embedment length led to an uneven stress distribution, resulting in lower ultimate bond stress values [14,28,31–34]. The relationship between bond stress and embedment length with various bar diameters of BFRP bars is summarized in Figures 9 and 10 below:

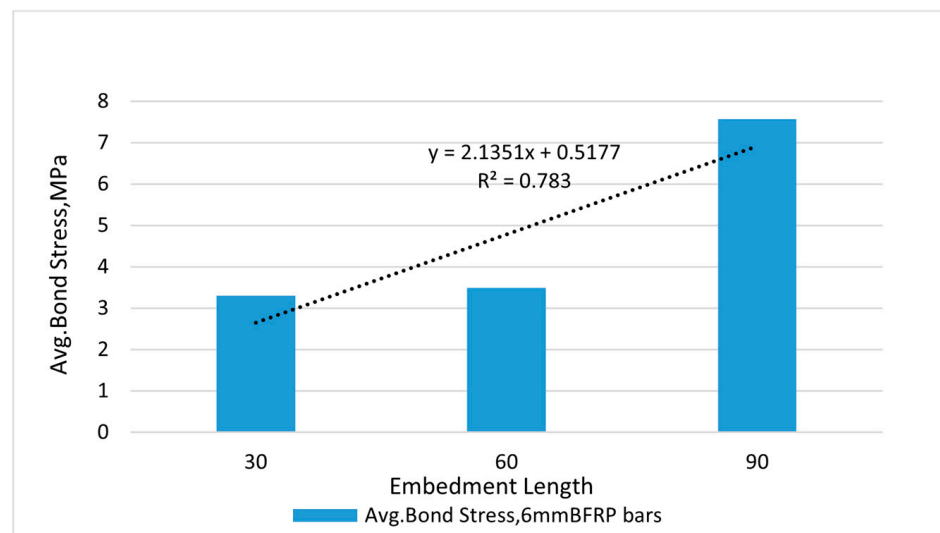


Figure 9. Average bond stress of 6-mm BFRP bars vs. embedment length.

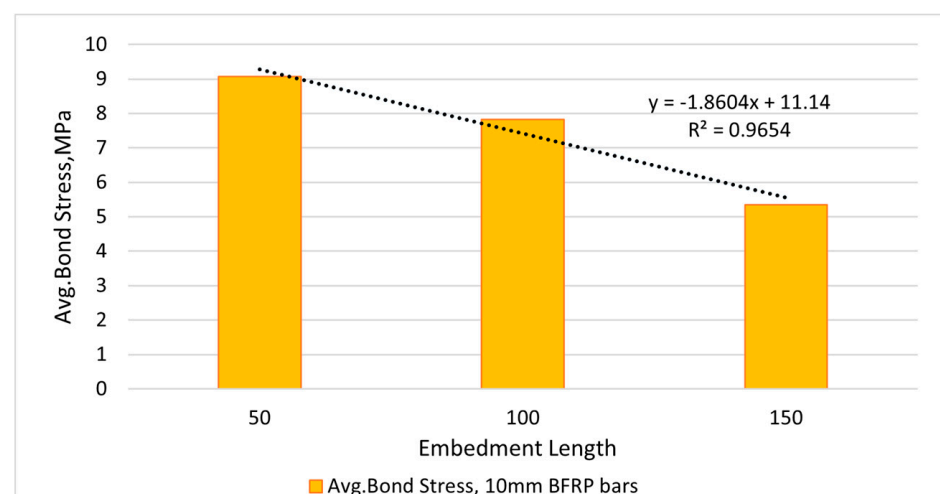


Figure 10. Average bond stress of 10-mm BFRP bars vs. embedment length.

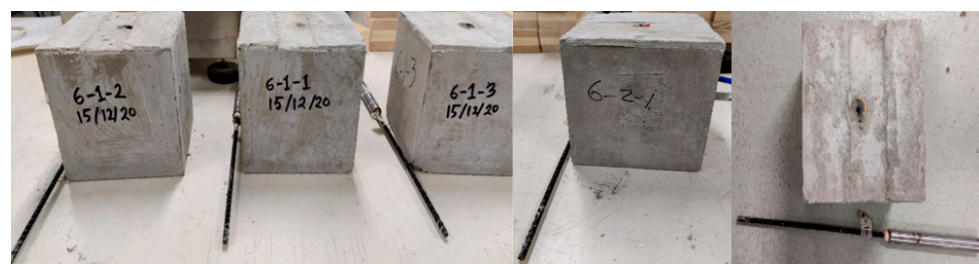
The decreased bond strength reported for the basalt FRP bars can also be attributed to the relatively smooth surface of the bars when compared to the deformed steel bars.

basalt FRP bars are a relatively new type of FRP bar whose material properties are still under investigation. Research on the bond performance of BFRP bars with various surface treatments—such as sand coating, helical wrapping, or ribbing with indentations—has been carried out by various researchers [2,35–38]. It has been found that providing sand coating increases the bond strength [35,38]; however, the sand coating has been found to separate from the core of the bar under severe exposure, such as that in marine environments [39]. The future direction of the current study aims at assessing the properties of BFRP bars under marine exposure conditions; hence, BFRP bars without any surface treatment were chosen.

3.2. Failure Mode

The failure modes commonly reported for the direct pull-out test by researchers are of three types [3,16,32,40]: The first type of failure is the pull-out failure, in which the bar under consideration pulls out of the concrete specimen under loading. The second type of failure is the splitting of the concrete; this type of failure is characterized by the cracking and breaking of the concrete even before the bars pull out under loading. The third type of failure is bar rupture, in which the reinforced bar yields or ruptures (in the case of FRP bars) and fails under loaded conditions [13]. Studies report that for reliable analysis of the bond performance with respect to bond strength, the expected type of failure is the pull-out of bars [41]. Pull-out failure is reported when the energy of the shearing bond strength between the bar and the geopolymer concrete exceeds the bonding capacity of the geopolymer concrete [42]. This gives a true depiction of the bond stresses acting on the pull-out specimens, and aids researchers in developing a better understanding of the bond performance of the composite structures [3,16,38]. It has been widely seen in previous research that the bond stress values reported for other types of failure, such as splitting of concrete or bar rupture, are often discarded in bond strength calculation owing to their inaccuracy in representing the bond stress distribution.

In this study, the predominant failure mode exhibited by all of the test specimens was pull-out failure, irrespective of the bar diameter or the embedment length. In the pull-out failures of this study, both the steel and BFRP bars pulled out from the embedded concrete under relatively low stress levels, with the bar surface showing a slightly worn rib for the steel bars, and a sheared-off, torn fibre rib surface in the case of BFRP bars. It can also be inferred that during loading, the concrete shears with the wound surface of the BFRP bars, and the bond surfaces start to get damaged due to continuous stress from the loaded end [32]. The embedment length then extends until the free end reaches the lowest point and causes a sudden excessive slip, resulting in the pull-out of the bars. This scenario is consistent with observations from recent studies in this field, and confirms the behaviour of basalt FRP under direct pull-out tests [38]. The failure damage images show that the bars pulled out of the specimens, and that the pull-out load could not be resisted by the bar–concrete interface owing to lowered adhesion due to the smooth surface of the BFRP bars against the surface of the SCGC [32,43,44]. The pull-out failures of the specimens of all of the series are shown in Figures 11–15.



Pull-Out failure of 6mm Basalt FRP bars

Figure 11. Pull-out failure of 6-mm BFRP bar specimens.



Figure 12. Pull-out failure of 10-mm basalt FRP bar specimens.

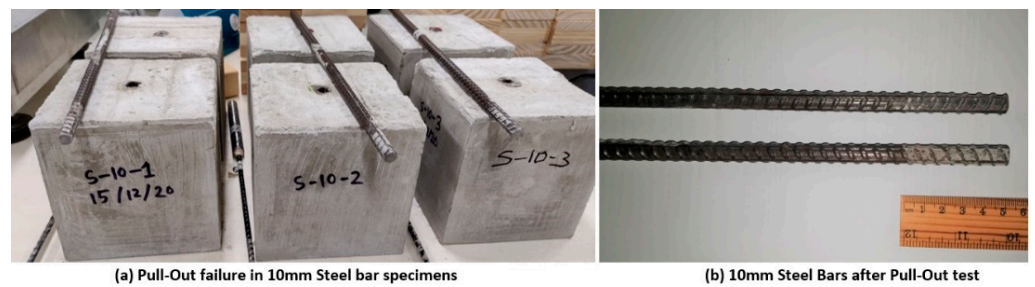


Figure 13. Pull-out failure of steel bar specimens.



Figure 14. Wear and tear on rib fibres on the pulled-out bar surface.

3.3. Effect of Bar Diameter and Embedment Length

It has been widely reported in the literature [18,19,36,40,41,45–48] that the bond strength decreases when there is an increase in the bar diameter, due to the non-linear distribution of stresses along the loaded end of the bar to the free end of the bar at the time of pull-out testing. Hence, in this study, two diameters of the basalt FRP bars—one belonging to the smaller diameter range (6 mm), and one belonging to the larger diameter range (10 mm)—have been selected.



Figure 15. Cross-sectional view of cut Pull-out specimens.

From the experimental observations, it is understood that the smaller diameter bars (6 mm) exhibited lower bond strength, which can be attributed to the early pull-out of the bars from the concrete matrices due to bonding failure. For the smaller diameter bars, even before reaching the peak stress values, the bar grip was loosened from the surrounding concrete, leading to early pull-out failure. The surface characteristics of the bar are another reason for this, as they are smooth when compared to the ribbed surfaces of the steel bars. The surface characteristics of the reinforced bars are of significance in direct pull-out studies, and it has been reported in many studies that a rougher surface—such as those in ribbed, sand-coated surfaces—offers better bonding due to friction in the bar–concrete interface [37,49,50].

Unlike the 6-mm bars, the bond stress of the 10-mm bars decreased with the increase in the bonded length, and was similar to that of steel rebars. The 10-mm BFRP and 10-mm steel rebars reported similar values of bond strength at an embedment length of 5 times the bar diameter. The cause of the decrease in bond stress with an increase of embedment length is attributed to the non-linear distribution of stresses along longer lengths [9,13,49,51].

The other variable used in this study is the embedment length (or development length), which is considered to be the length of the reinforcement bar required in any reinforced concrete structural element in order to provide sufficient bond strength between the reinforcement and the concrete [11,16,48,52]. The current study aims to identify the best suited embedment length when using basalt FRP reinforcement.

The bond stress values with respect to the different embedment length to bar diameter ratios (L/d_b) obtained from the tests are depicted in Figure 16 below:

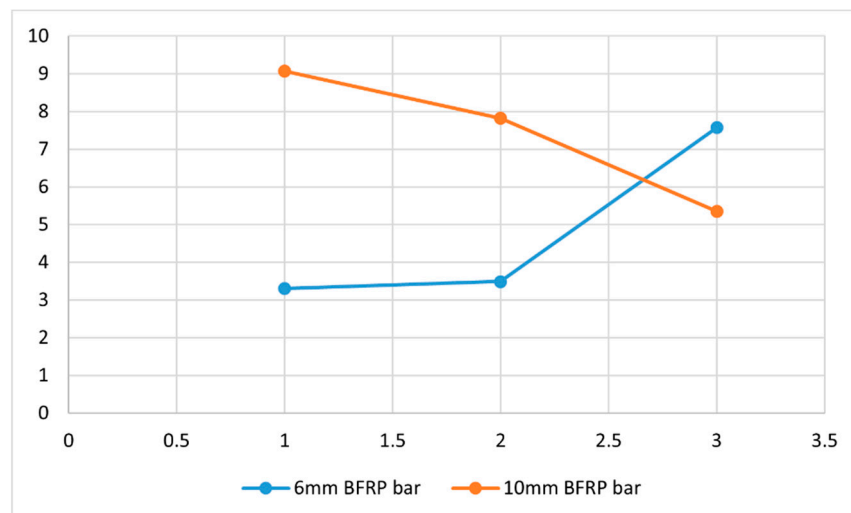


Figure 16. Bond stress vs. embedment length to bar diameter (L/d_b).

The basalt FRP bars of $5 d_b$ bonded length corresponding to an L/d_b ratio of 5 report higher bond strength when compared to L/d_b ratios of 10 and 15. There is a decrease in bond stress values for 10-mm bars when there is an increase in bond length, due to the non-linear distribution of stresses in the bars [38,53]. For the smaller 6-mm BFRP bars, the bond capacity of the concrete was very low even for longer embedment lengths, and the bars pulled out under peak loads as reported in a study by Michaud and Fam [16]. In the case of 6-mm bars, an embedment length of $15 d_b$ showed a slight increase in the bond strength; however, in all three embedment lengths, the peak load capacity of the 6-mm BFRP was not achieved.

Even though the only mode of failure reported in this study was the pull-out type, we observed that in specimens with $15 d_b$ embedment length, while the bar firstly pulled out of the SCGC, a crack of 1–2 mm width appeared on the top surface of the specimen immediately afterwards, as seen in Figure 17:

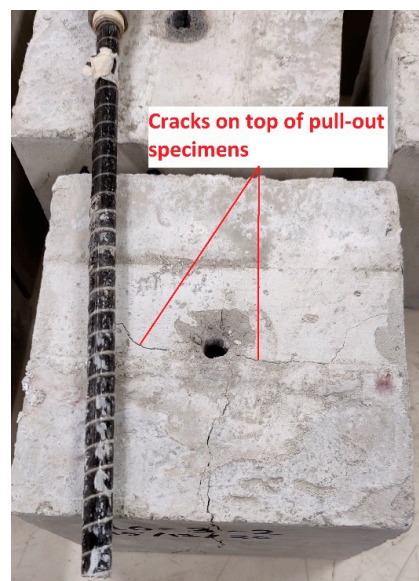


Figure 17. Crack on the top surface of the $15 d_b$ pull-out specimens.

3.4. Load–Slip Relationship

The slip of basalt FRP bars from the SCGC blocks was recorded throughout the test. The load–slip relationship for 6-mm bars of $5 d_b$, $10 d_b$, and $15 d_b$ is plotted in Figure 18 below:

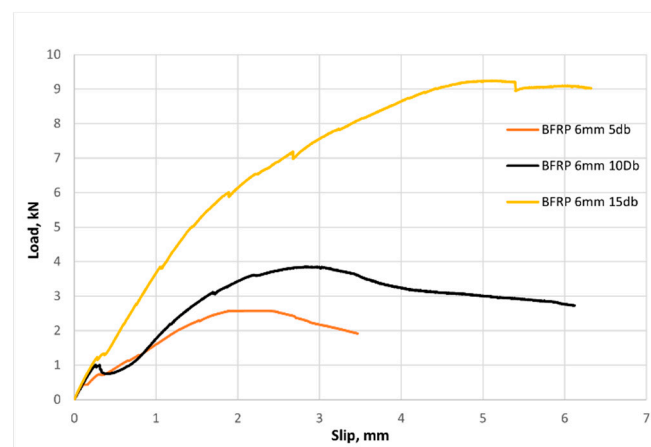


Figure 18. Load–slip relationship of specimens with 6-mm BFRP bars of $5 d_b$, $10 d_b$, and $15 d_b$ embedment lengths.

The specimens of 6-mm diameter of $5 d_b$ and $10 d_b$ embedment lengths pulled out from the concrete at early loading stages, even before reaching the peak stresses of the bar. When a larger embedment length of $15 d_b$ was used (Figure 22), the bond strength of the specimens showed an increase similar to that reported by Michaud and Fam in their study on BFRP bars in conventional concrete [16].

While observing the pull-out failure of 10-mm BFRP bars it was seen that the load taken by the 10-mm BFRP bars was higher than their 6-mm counterparts, and the bond strength was higher for smaller embedment lengths of $5 d_b$, as shown in the load–slip plot in Figure 19.

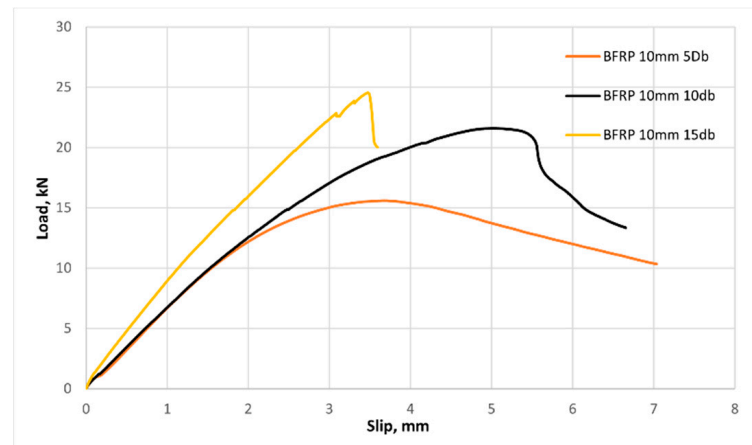


Figure 19. Load–slip relationship of specimens with 10-mm BFRP bars of $5 d_b$, $10 d_b$, and $15 d_b$ embedment lengths.

However, as the embedment length increased to $10 d_b$ and $15 d_b$, the ultimate failure load increased; however, the bond strength was smaller due to the non-uniform distribution of stresses over larger lengths of bond, leading to loss of grip from the concrete face and pull-out of bars. It is also of interest to note that in the longest embedment length ($15 d_b$) of BFRP bar, the bar pulled out before peak load, and the loading continued until splitting cracks were observed on the pull-out specimens.

The load–slip plot for the steel bars is shown in Figure 20 below, and the failure pattern was of pull-out type for all three specimens of the $5 d_b$ embedment length. However, for the first specimen (S-10-1), erroneous values were reported due to faulty running of the test machine, and these values were not considered for bond strength calculation.

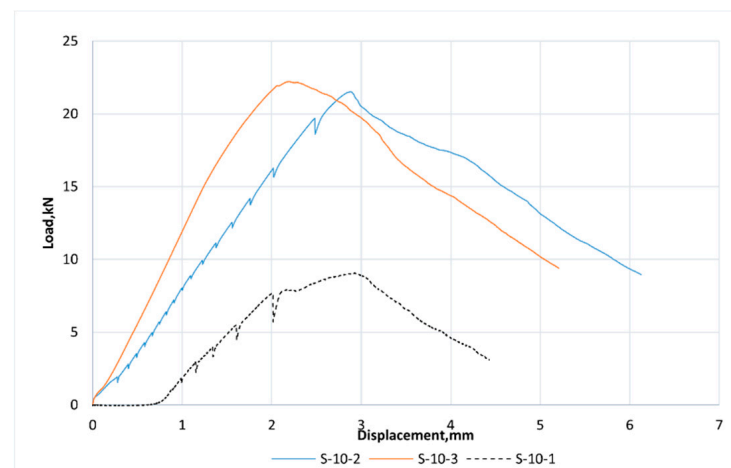


Figure 20. Load–slip relationship of the 10-mm, $5 d_b$ steel specimens.

The load–slip relationship comparing the performance of 6-mm BFRP bars of various embedment lengths ($5 d_b$, $10 d_b$, and $15 d_b$) against the performance of steel bars is also plotted below in Figure 21. In comparison to the steel bars, the BFRP bars of smaller diameter (i.e., 6 mm) could not perform well under pull-out test loads. Due to their smaller size and lower bond capacity, the bars pulled out of the concrete earlier, even before reaching the peak loads. The embedment length variations also did not make a difference in the bond strength capacities when compared to the steel bars, which performed well against the smaller diameter basalt FRP bars.

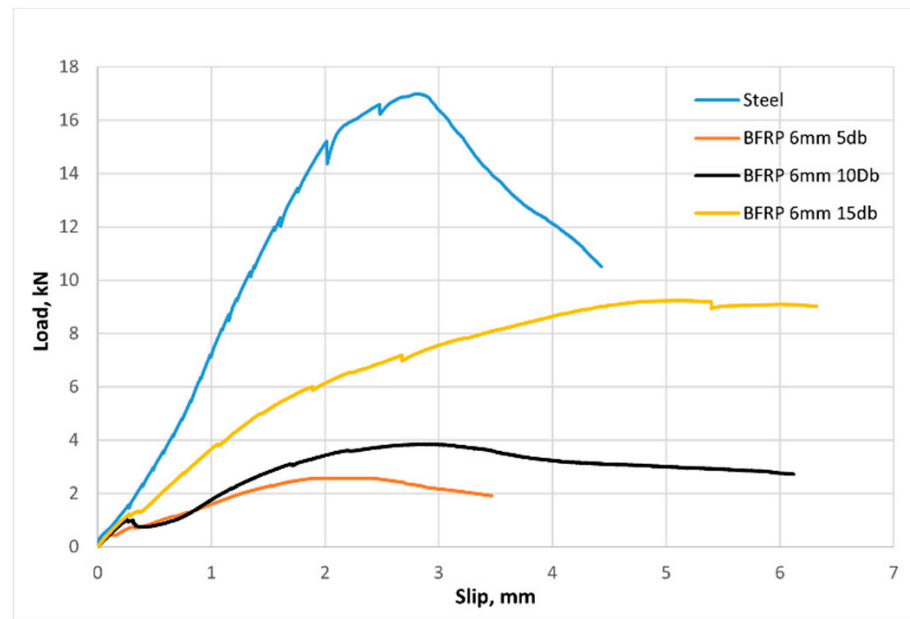


Figure 21. Load–slip relationship of the 6-mm BFRP and steel bars.

Moreover, the load–slip relationship comparing the performance of 10-mm BFRP bars of various embedment lengths ($5 d_b$, $10 d_b$, and $15 d_b$) against the performance of steel bars is also plotted below in Figure 22.

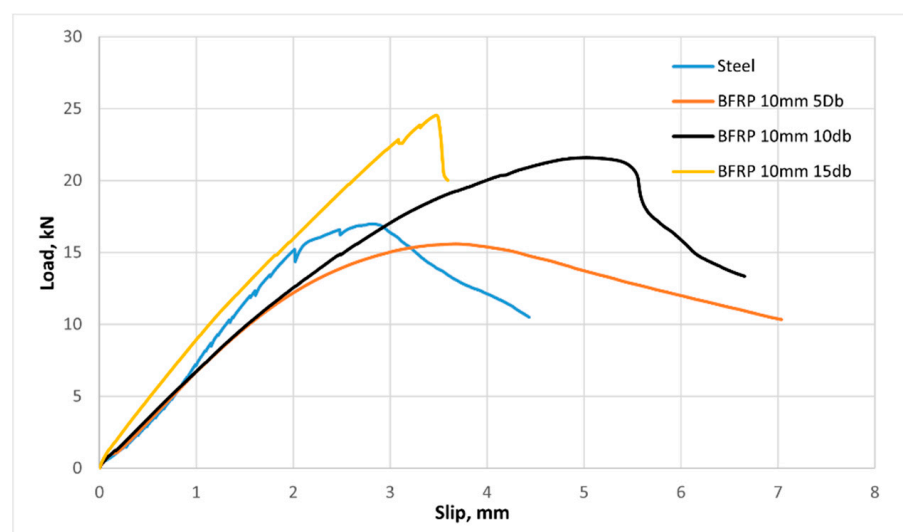


Figure 22. Load–slip relationship of the 10-mm BFRP and steel bars.

The peak loads of the 10-mm steel bars and 10-mm BFRP bars are in a similar range, confirming the suitability of BFRP bars as reinforcement materials, as can be seen from

the comparison plot in Figure 22. This indicates that the 10-mm bars of BFRP give similar pull-out performance when compared to steel bars of same diameter, showing promising potential for the use of Basalt FRP as an alternative for the conventional steel reinforcing bar. Furthermore, the results of specimens with steel bars were similar for self-compacting geopolymer concrete (SCGC), geopolymer concrete, and conventional concrete of 40 MPa strength [53–56]. The outlier values in some of the specimens in this series of experiments were due to the shutting down of the UTM midway through the experiment. This study provides promising results for the use of basalt bars as a reinforcement alternative to conventional steel bars. Moreover, the self-compacting geopolymer concrete, with its advantageous features—including strength, flowability, lack of need for vibration, and ambient curing properties—would make the BFRP-reinforced specimens more efficient to use easily in real life scenarios [1,2,7,53–56].

The current experimental investigation finds that while studying the causes of bond behaviour, it is important to consider other parameters, such as fibre volume in each of the bundles for basalt or any other kind of FRP bars, as these may influence the bond behaviour. The reinforcement sectional area, surface roughness of the rebar, bar diameter, and friction at the bar–concrete interface are other factors that have been found to affect the bond behaviour of pull-out specimens [19,52,57,58]. Bonding can also be affected by surface treatment of the bars, and by the country of origin/production of the bars. Hence, the results of this study hold true only for the current bar characteristics, and more studies are required to standardize basalt FRP bars' bond behaviour.

4. Theoretical Investigation of Bond Behaviour

The application of a new composite material in reinforcing concrete structures is highly dependent on the bond behaviour and strength, and specifically on the bar–concrete interaction in comparison to steel bars. Hence, knowledge of bond behaviour and other interfacial characteristics is vital to confirm a reliable transfer of forces in the reinforced structure. The commonly adopted tests by the ACI, Canadian, and other relevant standards include direct pull-out tests, notched beam tests, and push-out tests. Out of these tests, direct pull-out tests are the most commonly adopted, due to ease in test configuration. However, to confirm the bond characteristics, several parameters need to be studied. Analytical prediction models are used as an indicator in order to assess the bond properties of a possible configuration. The use of theoretical prediction models will help researchers in identifying the most critical parameters that affect overall behaviour. In the current study, the composite bars under consideration are basalt FRP bars embedded in a newly developed self-compacting geopolymer concrete, the behaviour of which is yet to be fully understood. Table 5 below lists the existing mathematical representations for steel and FRP bars in conventional concrete, which are currently adopted in ACI and CSA for the bond strength prediction of FRP bars [27,59,60].

Table 5. Bond strength prediction equation for FRP bars in concrete.

Sl.No:	Standard Guideline	Bond Strength Prediction Equation	FRP Bar Type	Remark
1	ACI 440.1R-06	$\tau_{\max} = 0.083\sqrt{f_c}(4.0 + 0.3c/d + 100d/l)$	Glass, E-glass, Carbon, Aramid	No specific coefficients of factors to account for the type and material of FRP bar
2	ACI 440.1R-03	$\tau_{\max} = 20.23\sqrt{f_c}/d$	Glass, E-glass, Carbon, Aramid	
3	CSA-S806-02	$\tau_{\max} = d_{cs} \sqrt{f_c} / 1.15(k_1 k_2 k_3 k_4 k_5)\pi d_b$	Glass, E-glass, Carbon, Aramid	Considers fibre type and profile of bar

τ_{\max} : bond strength; f_c : compressive strength of concrete; d_{cs} and c : concrete cover; d , d_b : bar diameter; l : embedment length; k_1 : bar location factor; k_2 : concrete density; k_3 : bar size factor; k_4 : bar fibre factor; k_5 : bar surface profile factor.

The theoretically predicted bond strength values, using the models above by ACI and CSA, are found to exaggerate the true bond behaviour, as depicted in Table 6 below:

Table 6. Comparison of experimental and predicted values of bond strength.

Specimen No.	Experimental Value of Bond Stress, MPa	Predicted Values of Bond Stress, MPa		
		ACI 440.1R-06 [3]	ACI440.1R-03 [4]	CSA S806-02 [5]
6-1-1	3.30	13.12	21.32	25.01
6-2-1	3.49	7.87	21.32	25.01
6-3-1	7.57	6.12	21.32	25.01
10-1-1	9.08	12.91	12.79	14.59
10-2-1	7.83	7.66	12.79	14.59
10-3-1	5.36	5.91	12.79	14.59

The comparison of the predicted values with the experimental values confirms the inadequacy of standards/design codes for accurately predicting the bond behaviour of a new FRP–geopolymer concrete composite. The only guidelines available for FRP bars in concrete—namely, the ACI [22,59] and CSA [27] guidelines—do not include basalt FRP bars or geopolymer concrete. The current practice is to use the same coefficients for glass FRP and BFRP bars, which creates non-conformity owing to differences in the material properties of glass and basalt fibres [18,61,62]. Numerous studies have focused on finding accurate coefficients corresponding to the type of FRP bar, material, and surface properties in order to produce an accurate prediction model [31,52,63]. However, it has been found that the developed mathematical models are not applicable to all the parameters affecting bond behaviour and performance [33,38,49].

The current paper thus identifies the need for a powerful learning technique, such as an artificial neural network (ANN), which can take into consideration an array of various parameters that can affect the bond performance of the FRP–SCGC composite. Unlike traditional prediction methods, the software supporting ANN learning tools is able to predict bond behaviour by considering the complex relationships amongst the various parameters and understanding the pattern of experimental results [64–66]. Thus, in the following section, artificial neural network tool performing under MATLAB 2020b software is used to develop the ANN model to predict the bond strength of BFRP bars in self-compacting geopolymer concrete.

4.1. Bond Strength Prediction Using an Artificial Neural Network (ANN)

The advent of various computational techniques incorporating artificial intelligence has helped researchers in different fields of study to better understand the complexity of datasets [65]. The artificial neural network (ANN) is a computational technique used for predicting and fitting complex datasets [61,67]. The ANN is unique from other methods due to its ability to learn like a human brain [64,68]. ANN predictions are thus considered to provide logical and intelligent solutions due to their self-learning capacity [61,65,68]. The architectural framework of an ANN consists of three main parts—namely, the input layer, hidden layer, and output layer [61,64,67]. The input layer consists of an input dataset where the different parameters for prediction are entered. In the hidden layer, there is a collection of nodes known as neurons, which represents the interrelationship between each of the input parameters [66,69]; this is the layer where mathematical computations are executed in order to provide the desired or targeted output in the output layer [61,68,70]. The neurons in the hidden layer can be assigned weights or bias in order to modify the targeted output, and are decided by learning and memorizing each input with the most desired output [71–73].

4.1.1. ANN Model Development

In this study, a backpropagation feed-forward neural network was used to develop the neural network fitting model. Since the model was developed after the experimental inves-

tigation, a backpropagation feed-forward neural network is best suited for developing the ANN model’s desired output, which was already obtained from the experimental results. The multilayered backpropagation network was created consisting of three layers—the input layer, the hidden layer with nodes, and the output layer—as shown in Figure 23 below:

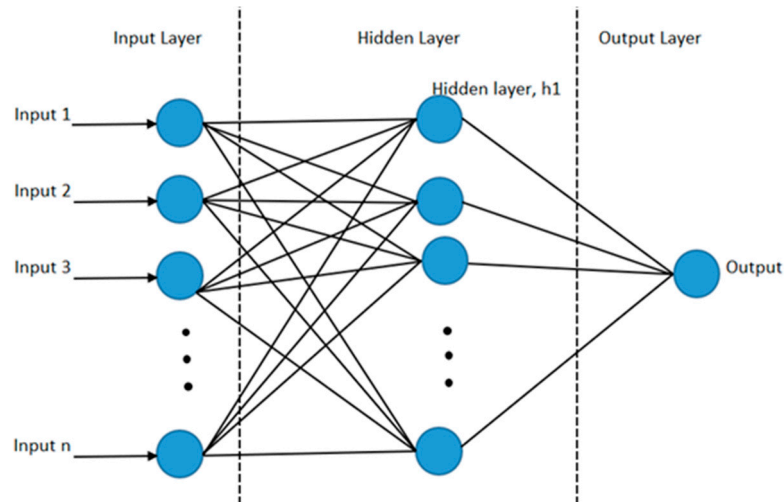


Figure 23. Artificial neural network architecture framework.

4.1.2. ANN Model Training and Analysis

Once the input parameters and target outputs were transformed to the form of numeric arrays called datasets, the training of the model was complete. In the current model, a supervised learning approach was carried out for the development of the model. The training of the data was conducted using the Levenberg–Marquardt optimization method, consisting of logistic sigmoid activation function in the hidden layer, as shown in Figure 24 below:

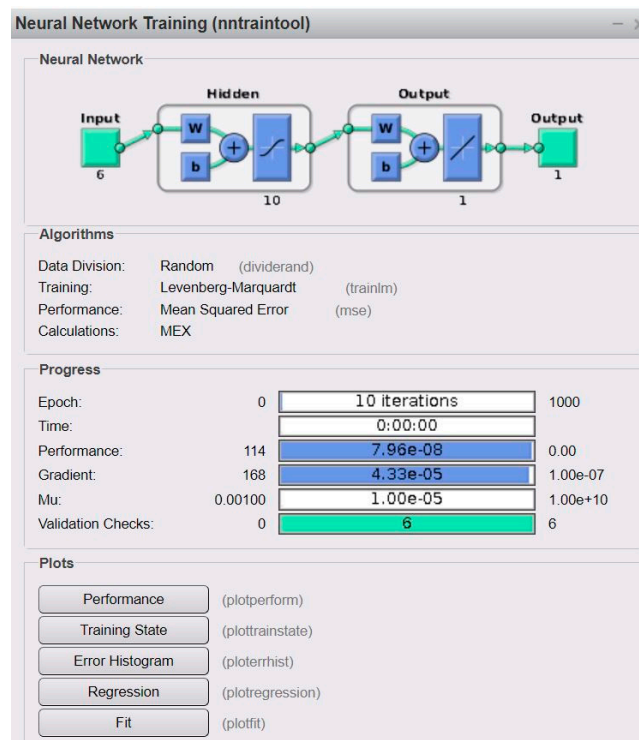


Figure 24. Neural network training.

Using the neural network fitting tool (nftool) in MATLAB, the input dataset consisting of six parameters—including compressive strength, bar diameter, cover/bar diameter ratio, embedment length/bar diameter, embedment length, and concrete—was fed to the model. This model uses 70% of the sample size for training of the model, and the remaining 30% for the validation and testing of the model, as shown in Figure 25 below:

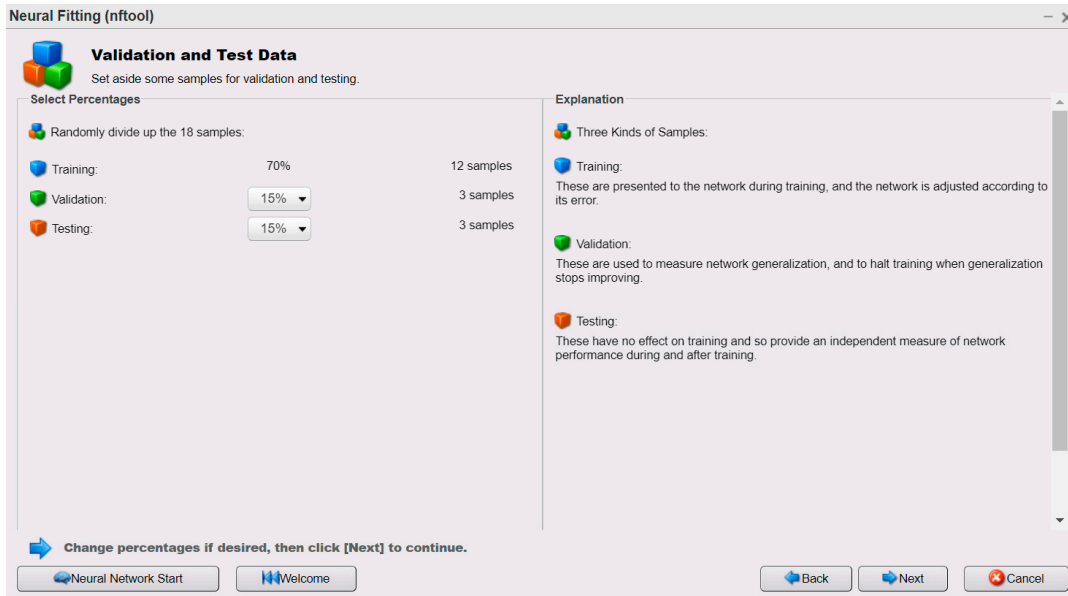


Figure 25. Neural fitting tool showing sample size.

The model was trained to obtain better predictability with correlation coefficients of 0.99, 0.96, and 0.97 for the training, validation, and test data, respectively, as shown in Figure 26 below:

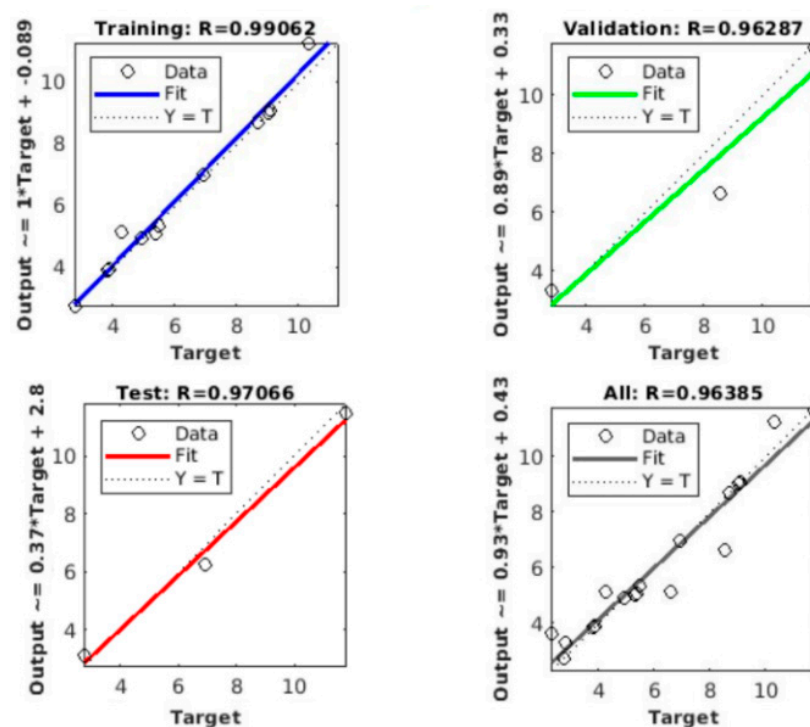


Figure 26. Regression plots for training, validation, and testing of the ANN model.

Figure 26 depicts the regression plots for the training, validation, and test datasets used by the ANN model, along with the validated result dataset. It is a screenshot of the plot drawn in the ANN model toolbox. The “Target” values in the X-Axis of the above plot refer to the experimental input values, and the Y-Axis output values correspond to the ANN-predicted values. Moreover, the vertical axes describe how output is calculated for each of the datasets used for the training, validation, and testing of the ANN model. From the regression plot, the accuracy of the model can be confirmed. This was obtained by training the network continually using the (nntraintool), which updates the weights until the mean squared error is small. However, repetitive training may cause the model to memorize the target values and result in overfitting of the model, and hence it is necessary to carry out regularization and identify the early fit during the training process [61,68,74]. Figure 27 below shows the best validation performance of the ANN model at epoch 4.

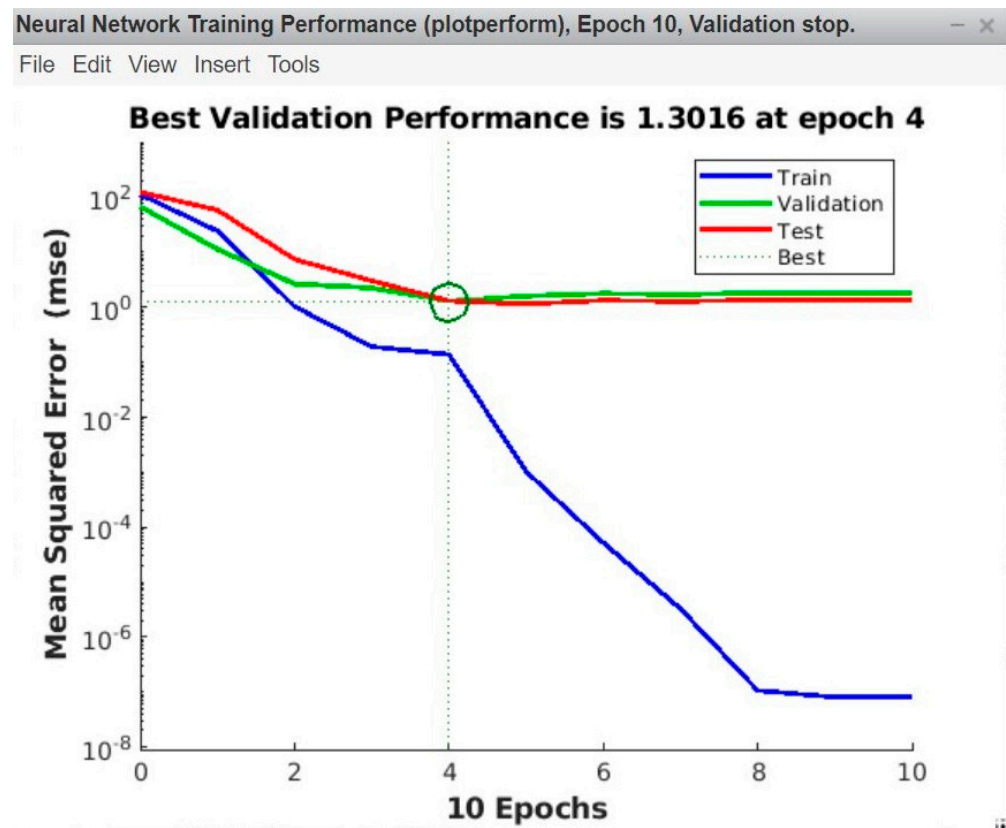


Figure 27. Validation Performance of the ANN Model.

4.2. ANN Comparison with Other Prediction Models

The predictive capability of the newly developed ANN model is compared initially with the experimental data, and the results show close agreement of bond strength values. The ANN model is also compared against prediction models recommended by the American Concrete Institute ACI 440.1R-03, ACI440.1R-06, and the Canadian Standard CSA S806-02 guidelines, and a comparison plot is shown in Figure 28 below.

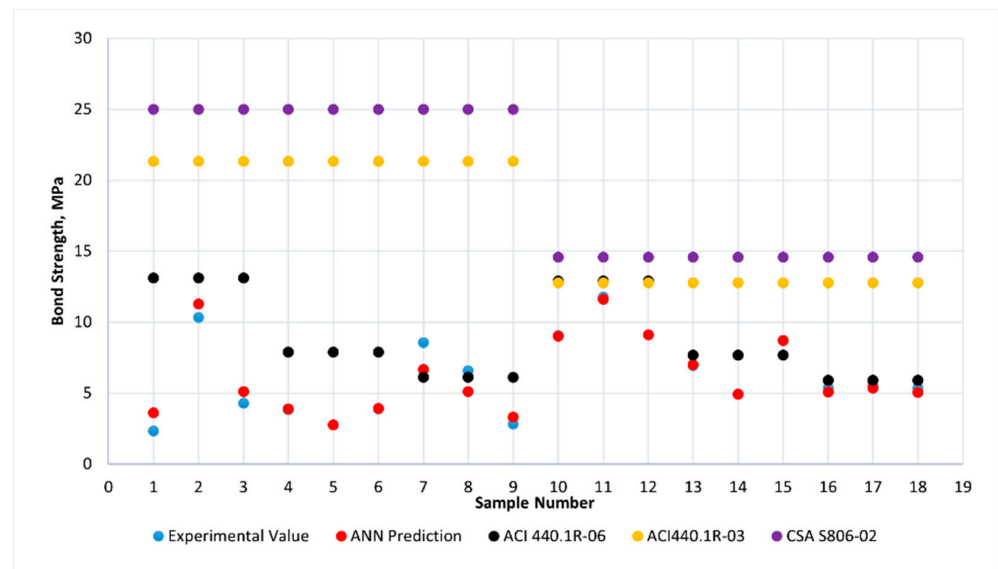


Figure 28. ANN model comparison against other prediction models for all specimens.

It is evident from the above plot that the ANN model is effective in predicting the bond strength of the basalt-FRP-reinforced SCGC specimens, and performs well against all of the other models. It can be seen that the ANN model is efficient in predicting smaller datasets with $R^2 = 0.96$, and can be trained with available sets of test data, providing better prediction for composites such as SCGC–BFRP that exhibit non-linear behaviour. This supports the use of ANN and similar computational techniques to predict this kind of dataset, with high randomness and irregularities. Unlike traditional mathematical models, there is no need for developing separate models, as ANNs provide a good fit for randomized data using intelligent algorithms.

5. Conclusions

In this study, the bond behaviour of basalt-FRP-reinforced, newly developed self-compacting geopolymer concrete was investigated by conducting direct pull-out tests on 21 specimens under ambient-cured conditions. These testing conditions were used in other bond behaviour studies reported in the literature, where the samples were air cured in the same laboratory environmental conditions ($23 \pm 2^\circ\text{C}$ and relative humidity of 50%) [75,76]. The results of the current study are consistent with other reported studies, where the air-cured specimens displayed promising bond performance for specimens reinforced with FRP bars or FRP sheets [75,76]. This study considered bar diameter and embedment length as the variable parameters, and compared them against the performance of steel rebar under similar conditions. This study also took into consideration the type of bar, compressive strength, and concrete cover in assessing the influence of various parameters affecting bond performance. From the test results it could be concluded that:

1. The average bond strength offered by 10-mm steel-reinforced SCGC is higher than that of 6-mm and 10-mm BFRP bars; however, all of the BFRP-reinforced specimens gave similar bond performance for traditional, ordinary Portland cement concrete.
2. The 10-mm-diameter BFRP bars performed well when the embedment length was kept at $5 d_b$, and when the embedment length was increased, the bond strength was found to decrease for 10-mm BFRP bars.
3. When comparing the performance of basalt bars with steel bars, we noted that the pull-out specimens reinforced with steel were able to take maximum stresses (around 500 MPa); however, for the basalt, since the tensile stress was almost 1100 MPa, the basalt bars pulled out before the peak was reached.
4. Even though the ANN model is a non-traditional approach, it proved to provide realistic prediction in the case of the newly developed composite (SCGC–BFRP) com-

pared to the existing theoretical and analytical models, such as ACI and CSA, which overpredicted the bond strength.

5. The ANN model gave good prediction of bond strength, with the lowest MSE values, and R^2 values of 0.99 for test, 0.97 for validation and 0.96 for training for all types of basalt FRP specimens. Future works on this topic would enhance the database to give more accurate predictions.

Author Contributions: S.K.R.: methodology, investigation, writing—original draft; R.A.-A.: supervision, writing—review and editing. All authors have read and agreed to the published version of the manuscript.

Funding: This research received no external funding.

Institutional Review Board Statement: Not applicable.

Informed Consent Statement: Not applicable.

Data Availability Statement: Data are available upon request from the corresponding author.

Acknowledgments: The authors gratefully acknowledge the technical staff—Ikramul Kabir and Lube Veljanoski—for their support and assistance in completing the experimental investigations at the Structures Laboratory, Deakin University.

Conflicts of Interest: The authors declare no conflict of interest.

References

1. Rolland, A.; Quiertant, M.; Khadour, A.; Chataigner, S.; Benzarti, K.; Argoul, P. Experimental investigations on the bond behavior between concrete and FRP reinforcing bars. *Constr. Build. Mater.* **2018**, *173*, 136–148. [[CrossRef](#)]
2. Dong, Z.; Wu, G.; Xu, B.; Wang, X.; Taerwe, L. Bond durability of BFRP bars embedded in concrete under seawater conditions and the long-term bond strength prediction. *Mater. Des.* **2016**, *92*, 552–562. [[CrossRef](#)]
3. Zheng, Y.; Zhou, N.; Zhou, L.; Zhang, H.; Li, H.; Zhou, Y. Experimental and theoretical study of bond behaviour between FRP bar and high-volume fly ash-self-compacting concrete. *Mater. Struct.* **2021**, *54*, 1–17. [[CrossRef](#)]
4. Alkhraisha, H.; Mhanna, H.; Tello, N.; Abed, F. Serviceability and flexural behavior of concrete beams reinforced with basalt fiber-reinforced polymer (BFRP) Bars Exposed to Harsh Conditions. *Polymers* **2020**, *12*, 2110. [[CrossRef](#)] [[PubMed](#)]
5. El Mesalami, N.; Abed, F.; El Refai, A. Concrete columns reinforced with GFRP and BFRP bars under concentric and eccentric loads: Experimental testing and analytical investigation. *J. Compos. Constr.* **2021**, *25*, 04021003. [[CrossRef](#)]
6. Kashani, A.; Ngo, T.D.; Mendis, P. The effects of precursors on rheology and self-compactness of geopolymer concrete. *Mag. Concr. Res.* **2019**, *71*, 557–566. [[CrossRef](#)]
7. Ranjbar, N.; Zhang, M. Fiber-reinforced geopolymer composites: A review. *Cem. Concr. Compos.* **2020**, *107*, 103498. [[CrossRef](#)]
8. Rahman, S.K.; Al-Ameri, R. A newly developed self-compacting geopolymer concrete under ambient condition. *Constr. Build. Mater.* **2021**, *267*, 121822. [[CrossRef](#)]
9. Desnerck, P.; de Schutter, G.; Taerwe, L. Bond behaviour of reinforcing bars in self-compacting concrete: Experimental determination by using beam tests. *Mater. Struct. Constr.* **2010**, *43*, 53–62. [[CrossRef](#)]
10. Boel, V.; Helinckx, P.; Desnerck, P.; De Schutter, G. Bond Behaviour and shear capacity of self-compacting concrete. In *Design, Production and Placement of Self-Consolidating Concrete*; Springer: Dordrecht, The Netherlands, 2010; pp. 343–353.
11. Tighiouart, B.; Benmokrane, B.; Gao, D. Investigation of bond in concrete member with fibre reinforced polymer (FRP) bars. *Constr. Build. Mater.* **1998**, *12*, 453–462. [[CrossRef](#)]
12. FIB. *FRP Reinforcement in RC Structures*; Technical Report, Bulletin No. 40; FIB: Lausanne, Switzerland, 2007.
13. High, C.; Seliem, H.M.; El-Safty, A.; Rizkalla, S.H. Use of basalt fibers for concrete structures. *Constr. Build. Mater.* **2015**, *96*, 37–46. [[CrossRef](#)]
14. Elgabbas, F.; Vincent, P.; Ahmed, E.A.; Benmokrane, B. Experimental testing of basalt-fiber-reinforced polymer bars in concrete beams. *Compos. Part B Eng.* **2016**, *91*, 205–218. [[CrossRef](#)]
15. Ahmed, A.; Guo, S.; Zhang, Z.; Shi, C.; Zhu, D. A review on durability of fiber reinforced polymer (FRP) bars reinforced seawater sea sand concrete. *Constr. Build. Mater.* **2020**, *256*, 119484. [[CrossRef](#)]
16. Michaud, D.; Fam, A. Development length of small-diameter basalt FRP bars in normal- and high-strength concrete. *J. Compos. Constr.* **2021**, *25*, 04020086. [[CrossRef](#)]
17. Ceroni, F.; Cosenza, E.; Gaetano, M.; Pecce, M.R. Durability issues of FRP rebars in reinforced concrete members. *Cem. Concr. Compos.* **2006**, *28*, 857–868. [[CrossRef](#)]
18. Cosenza, E.; Manfredi, G.; Realfonzo, R. Behavior and modeling of bond of FRP rebars to concrete. *J. Compos. Constr.* **1997**, *1*, 40–51. [[CrossRef](#)]

19. Nanni, A.; Faza, S. Design and construction of concrete reinforced with FRP bars: An emerging technology. *Concr. Int.* **2002**, *24*, 53–58.
20. Mesbah, H.-A.; Benzaid, R.; Benmokrane, B. Evaluation of bond strength of FRP reinforcing rods in concrete and FE modelling. *Int. J. Civ. Eng. Constr. Sci.* **2017**, *4*, 21–41.
21. Khayat, K.H.; Desnerck, P. Bond properties of self-compacting concrete. In *Mechanical Properties of Self-Compacting Concrete; State-of-the-Art Report of RILEM Technical Committee 228-MPS*; Springer: Cham, Switzerland, 2014; pp. 95–139.
22. ACI Committee. *Guide Test Methods for Fiber-Reinforced Polymer (FRP) Composites for Reinforcing or Strengthening Concrete and Masonry Structures*; ACI 440.3R-04; ACI: Farmington Hills, MI, USA, 2012.
23. RILEM. *RILEM Technical Recommendations for the Testing and Use of Construction Materials*; RILEM: Paris, France, 1994.
24. Shoaib Hussain, A.; Al-Ameri, R. *Bond Strength and Anchorage Length of BFRP in Concrete*; Deakin University: Geelong, Australia, 2019.
25. Domone, P.L.; Chai, H.W. Design and testing of self-compacting concrete. In *Production Methods and Workability of Concrete*; CRC Press: Boca Raton, FL, USA, 2020.
26. Chopra, D.; Siddique, R. Kunal Strength, permeability and microstructure of self-compacting concrete containing rice husk ash. *Biosyst. Eng.* **2015**, *130*, 72–80. [[CrossRef](#)]
27. CSA. *Design and Construction of Building Components with Fibre-Reinforced Polymers*; CSA: Toronto, ON, USA, 2002.
28. Wang, L.; Song, Z.; Yi, J.; Li, J.; Fu, F.; Qian, K. Experimental studies on bond performance of BFRP bars reinforced coral aggregate concrete. *Int. J. Concr. Struct. Mater.* **2019**, *13*, 1–10. [[CrossRef](#)]
29. Nguyen, H.-A.; Chang, T.-P.; Shih, J.-Y. Engineering properties and bonding behavior of self-compacting concrete made with no-cement binder. *J. Mater. Civ. Eng.* **2018**, *30*, 04017294. [[CrossRef](#)]
30. Castel, A.; Foster, S.J. Bond strength between blended slag and Class F fly ash geopolymer concrete with steel reinforcement. *Cem. Concr. Res.* **2015**, *72*, 48–53. [[CrossRef](#)]
31. Liu, H.; Yang, J.; Wang, X. Bond behavior between BFRP bar and recycled aggregate concrete reinforced with basalt fiber. *Constr. Build. Mater.* **2017**, *135*, 477–483. [[CrossRef](#)]
32. Trabacchin, G.; Ayala, D.D.; Stegemann, J.; Zhang, M. Bond behaviour of basalt FRP bars in geopolymer concrete bond behaviour of basalt FRP bars in geopolymer concrete. In *Proceedings of the 1st International Conference in Low-Carbon Cement & Concrete Technology*, London, UK, 24–26 June 2019; pp. 1–4.
33. El Refai, A.; Ammar, M.-A.; Masmoudi, R. Bond performance of basalt fiber-reinforced polymer bars to concrete. *J. Compos. Constr.* **2015**, *19*, 04014050. [[CrossRef](#)]
34. Shen, D.; Li, C.; Feng, Z.; Wen, C.; Ojha, B. Influence of strain rate on bond behavior of concrete members reinforced with basalt fiber-reinforced polymer rebars. *Constr. Build. Mater.* **2019**, *228*, 116755. [[CrossRef](#)]
35. Solyom, S.; Balázs, G.L. Bond of FRP bars with different surface characteristics. *Constr. Build. Mater.* **2020**, *264*, 119839. [[CrossRef](#)]
36. Muñoz, M.B. Study of Bond Behaviour between FRP Reinforcement and Concrete. Ph.D. Thesis, Universitat de Girona, Girona, Spain, 2010.
37. Vincent, P.; Ahmed, E.; Benmokrane, B. Characterization of basalt fiber-reinforced polymer (BFRP) reinforcing bars for concrete structures. In *Proceedings of the 3rd Specialty Conference on Material Engineering & Applied Mechanics*, Canadian Society of Civil Engineers, Montreal, QC, Canada, 29 May–1 June 2013.
38. Liu, X.; Wang, X.; Xie, K.; Wu, Z.; Li, F. Bond behavior of basalt fiber-reinforced polymer bars embedded in concrete under mono-tensile and cyclic loads. *Int. J. Concr. Struct. Mater.* **2020**, *14*, 1–15. [[CrossRef](#)]
39. Dong, Z.; Wu, G.; Zhao, X.-L.; Wang, Z.-K. A refined prediction method for the long-term performance of BFRP bars serviced in field environments. *Constr. Build. Mater.* **2017**, *155*, 1072–1080. [[CrossRef](#)]
40. Baena, M.; Torres, L.; Turon, A.; Barris, C. Experimental study of bond behaviour between concrete and FRP bars using a pull-out test. *Compos. Part B Eng.* **2009**, *40*, 784–797. [[CrossRef](#)]
41. Maranan, G.; Manalo, A.; Karunasena, K.; Benmokrane, B. Bond stress-slip behavior: Case of GFRP bars in geopolymer concrete. *J. Mater. Civ. Eng.* **2015**, *27*, 04014116. [[CrossRef](#)]
42. Bi, Q.; Wang, H. Bond strength of BFRP bars to basalt fiber reinforced high-strength concrete. In *Advances in FRP Composites in Civil Engineering, Proceedings of the 5th International Conference on FRP Composites in Civil Engineering, CICE, Beijing, China, 27–29 September 2010*; Springer: Berlin/Heidelberg, Germany, 2011.
43. Seis, M.; Beycioğlu, A. Bond performance of basalt fiber-reinforced polymer bars in conventional Portland cement concrete: A relative comparison with steel rebar using the hinged beam approach. *Sci. Eng. Compos. Mater.* **2017**, *24*, 909–918. [[CrossRef](#)]
44. Golareshani, E.M.; Rahai, A.; Sebt, M.H. Bond behavior of steel and GFRP bars in self-compacting concrete. *Constr. Build. Mater.* **2014**, *61*, 230–240. [[CrossRef](#)]
45. Achillides, Z.; Pilakoutas, K. Bond behavior of fiber reinforced polymer bars under direct pullout conditions. *J. Compos. Constr.* **2004**, *8*, 173–181. [[CrossRef](#)]
46. Elgabbas, F.; Ahmed, E.A.; Benmokrane, B. Physical and mechanical characteristics of new basalt-FRP bars for reinforcing concrete structures. *Constr. Build. Mater.* **2015**, *95*, 623–635. [[CrossRef](#)]
47. Teffers, R.; De Lorenzis, L. Bond of FRP reinforcement in concrete—A challenge. *Mech. Compos. Mater.* **2003**, *39*, 315–328. [[CrossRef](#)]

48. Cosenza, E.; Manfredi, G.; Realfonzo, R. Development length of FRP straight rebars. *Compos. Part B Eng.* **2002**, *33*, 493–504. [[CrossRef](#)]
49. Wambeke, B.W.; Shield, C.K. Development length of glass fiber-reinforced polymer bars in concrete. *ACI Struct. J.* **2006**, *103*, 11.
50. Hong, L.; Chen, Y.D.; Li, T.D.; Gao, P.; Sun, L.Z. Microstructure and bonding behavior of fiber-mortar interface in fiber-reinforced concrete. *Constr. Build. Mater.* **2020**, *232*, 117235. [[CrossRef](#)]
51. Hong, L.; Li, T.; Chen, Y.; Gao, P.; Sun, L. Characteristics of interfacial shear bonding between basalt fiber and Mortar Matrix. *Materials* **2020**, *13*, 5037. [[CrossRef](#)] [[PubMed](#)]
52. Mousavi, S.; Dehestani, M. Bond strength and development length of glass fiber-reinforced polymer bar in unconfined self-consolidating concrete. *J. Reinf. Plast. Compos.* **2016**, *35*, 924–941. [[CrossRef](#)]
53. Nurwidayati, R.; Ekaputri, J.J.; Triwulan; Suprobo, P. Effect of embedment length on bond strength of geopolymer concrete. In *AIP Conference Proceedings*; AIP Publishing: College Park, MD, USA, 2020.
54. Hamad, J.A.R.; Johari, M.A.M.; Haddad, R.H. Mechanical properties and bond characteristics of different fiber re-inforced polymer rebars at elevated temperatures. *Constr. Build. Mater.* **2017**, *142*, 521–535. [[CrossRef](#)]
55. Looney, T.J.; Arezoumandi, M.; Volz, J.S.; Myers, J.J. An experimental study on bond strength of reinforcing steel in self-consolidating concrete. *Int. J. Concr. Struct. Mater.* **2012**, *6*, 187–197. [[CrossRef](#)]
56. Saleh, N.; Ashour, A.; Lam, D.; Sheehan, T. Experimental investigation of bond behaviour of two common GFRP bar types in high—Strength concrete. *Constr. Build. Mater.* **2019**, *201*, 610–622. [[CrossRef](#)]
57. Islam, S.; Afeiy, H.M.; Sennah, K.; Azimi, H. Bond characteristics of straight- and headed-end, ribbed-surface, GFRP bars embedded in high-strength concrete. *Constr. Build. Mater.* **2015**, *83*, 283–298. [[CrossRef](#)]
58. Maranan, G.B.; Manalo, A.C.; Karunasena, W.; Benmokrane, B. Pullout behaviour of GFRP bars with anchor head in geo-polymer concrete. *Compos. Struct.* **2015**, *132*, 1113–1121. [[CrossRef](#)]
59. ACI (American Concrete Institute). *Guide for the Design and Construction of Structural Concrete Reinforced with Fiber-Reinforced Polymer (FRP) Bars*; ACI 440.1R-15; ACI: Farmington Hills, MI, USA, 2015.
60. ACI (American Concrete Institute). *Guide for the Design and Construction of Concrete Reinforced with FRP Bars*; ACI 440.1R-03; ACI: Farmington Hills, MI, USA, 2003.
61. Haddad, R.; Haddad, M. Predicting fiber-reinforced polymer-concrete bond strength using artificial neural networks: A comparative analysis study. *Struct. Concr.* **2021**, *22*, 38–49. [[CrossRef](#)]
62. He, Z.; Tian, G.-W. Probabilistic evaluation of the design development length of a GFRP rod pull-out from concrete. *Eng. Struct.* **2011**, *33*, 2943–2952. [[CrossRef](#)]
63. Acciai, A.; D’Ambrisi, A.; De Stefano, M.; Feo, L.; Focacci, F.; Nudo, R. Experimental response of FRP reinforced members without transverse reinforcement: Failure modes and design issues. *Compos. Part B Eng.* **2016**, *89*, 397–407. [[CrossRef](#)]
64. Gao, J.; Koopialipour, M.; Armaghani, D.J.; Ghabussi, A.; Baharom, S.; Morasaei, A.; Shariati, A.; Khorami, M.; Zhou, J. Evaluating the bond strength of FRP in concrete samples using machine learning methods. *Smart Struct. Syst.* **2020**, *26*, 403–418.
65. Dahou, Z.; Sbartaï, Z.M.; Castel, A.; Ghomari, F. Artificial neural network model for steel–concrete bond prediction. *Eng. Struct.* **2009**, *31*, 1724–1733. [[CrossRef](#)]
66. Makni, M.; Daoud, A.; Karray, M.A.; Lorrain, M. Artificial neural network for the prediction of the steel-concrete bond behaviour. *Eur. J. Environ. Civ. Eng.* **2014**, *18*, 862–881. [[CrossRef](#)]
67. Golafshani, E.M.; Rahai, A.; Sebt, M.H. Artificial neural network and genetic programming for predicting the bond strength of GFRP bars in concrete. *Mater. Struct.* **2014**, *48*, 1581–1602. [[CrossRef](#)]
68. Su, M.; Zhong, Q.; Peng, H.; Li, S. Selected machine learning approaches for predicting the interfacial bond strength between FRPs and concrete. *Constr. Build. Mater.* **2021**, *270*, 121456. [[CrossRef](#)]
69. George, U.A.; Elvis, M.M. Modelling of the mechanical properties of concrete with cement ratio partially replaced by aluminium waste and sawdust ash using artificial neural network. *SN Appl. Sci.* **2019**, *1*, 1514. [[CrossRef](#)]
70. Bashir, R.; Ashour, A. Neural network modelling for shear strength of concrete members reinforced with FRP bars. *Compos. Part B Eng.* **2012**, *43*, 3198–3207. [[CrossRef](#)]
71. Alnedawi, A.; Al-Ameri, R.; Nepal, K.P. Neural network-based model for prediction of permanent deformation of unbound granular materials. *J. Rock Mech. Geotech. Eng.* **2019**, *11*, 1231–1242. [[CrossRef](#)]
72. Sancak, E. Prediction of bond strength of lightweight concretes by using artificial neural networks. *Sci. Res. Essays* **2009**, *30*, 256–266.
73. Abdalla, J.A.; Hawileh, R.; Altamimi, A.K. Prediction of FRP-concrete ultimate bond strength using Artificial Neural Network. In *Proceedings of the 4th International Conference on Modeling, Simulation and Applied Optimization (ICMSAO)*, Kuala Lumpur, Malaysia, 19–21 April 2011; pp. 1–4.
74. Asteris, P.; Kolovos, K.; Douvika, M.; Roinos, K. Prediction of self-compacting concrete strength using artificial neural networks. *Eur. J. Environ. Civ. Eng.* **2016**, *20*, s102–s122. [[CrossRef](#)]
75. Ceroni, F.; Bonati, A.; Galimberti, V.; Occhiuzzi, A. Effects of Environmental Conditioning on the Bond Behavior of FRP and FRCM Systems Applied to Concrete Elements. *J. Eng. Mech.* **2018**, *144*, 04017144. [[CrossRef](#)]
76. De Domenico, D.; Urso, S.; Borsellino, C.; Spinella, N.; Recupero, A. Bond behavior and ultimate capacity of notched concrete beams with externally-bonded FRP and PBO-FRCM systems under different environmental conditions. *Constr. Build. Mater.* **2020**, *265*, 121208. [[CrossRef](#)]